16

Propagation of Electromagnetic Waves in and around Plasmas

Osamu Sakai
Kyoto University
Japan

1. Introduction

1.1 Historical perspective

Interaction between electromagnetic waves and plasmas has been explored for several decades in various fields, such as ionosphere layers and outer space (Ginzburg, 1964), fusion plasmas (Stix, 1962; Swanson, 1989; Nishikawa & Wakatani, 1990), and plasma material-processing reactors (Lieberman & Lichtenberg, 1994). When an electromagnetic wave is launched in or near a non-magnetized plasma whose size is much larger than the wavelength, it is transmitted, reflected, or absorbed; these features are determined by a set of the electromagnetic wave frequency, the electron plasma frequency, and the electron elastic collision frequency. These three parameters determine real and imaginary parts of permittivity. In other words, plasmas equivalently behave as conductors or dielectric materials for electromagnetic waves, and these behaviours are controllable by changing complex permittivity, or electron density and gas pressure, which is associated with the electron plasma frequency and the electron elastic collision frequency; this controllability and the time-varying manner for permittivity distinguish plasmas from other electromagnetic media.

First of all, in this section, we briefly review the historical perspective of the electromagnetic waves in plasmas, and we point out the reasons why the concept of electromagnetic media composed of plasmas and their discontinuities is focused on in this chapter.

Electromagnetic waves in magnetized plasmas have been well investigated for more than half century, aiming at ultimate goals of controlled fusion plasmas for energy production and space plasmas for launching human beings using spacecrafts. In a magnetized plasma, various kinds of wave branches are present from low to high frequency ranges, and change of the external magnetic field induces "walk" on the dispersion curves in a "zoo" of plasma waves. Sometimes a branch leads to another totally-different branch; that is called mode conversion (Stix, 1962; Swanson, 1989). These waves can be launched from the outer side of the plasma, but there are also many inherent waves found as magnetohydrodynamic and micro instabilities (Swanson, 1989; Nishikawa & Wakatani, 1990). Other characteristic features of plasma waves are their nonlinearity; shock waves, solitons, and nonlinear mode conversion originate from the aspects of high-energy-state substance (Swanson 1989). The main focus in this chapter is different from such conventional scientific interests.

Before we start our description, one more comment about plasma production for industry should be addressed (Lieberman & Lichtenberg, 1994). Plasma production in fabrication

processes of thin film technology was quite successful, and several different methods have been developed for semiconductor industry, flat panel display markets, and photovoltaic cell production. Such a technology using plasmas is now somewhat mature, and several different ideas and schemes for researches on plasma science and engineering are being tested for other applicable fields.
In such a sense, we study new types of plasma-wave interactions, especially arising from discontinuities in both space and time. Progress of techniques to control shape and parameters of plasmas enables us to make discontinuities in a clear and stable state.

1.2 Emerging aspects of plasma wave propagation

Since wave propagation in a magnetized plasma is well described elsewhere (Stix, 1962; Ginzburg, 1964; Swanson 1989), we here focus on the propagation in and around a non-magnetized plasma. It is not so complicated to describe electromagnetic waves propagating in and around a bulk non-magnetized plasma (Kalluri, 1998), although the propagation in a spatially-nonuniform plasma, in which electron-density gradient is significant (Swanson, 1989; Nickel et al., 1963; Sakai et al., 2009) and/or the profiles of electron density is spatially periodic (Hojo & Mase, 2004; Sakai et al., 2005(1); Sakai et al., 2005(2); Sakai et al., 2007(1); Sakai et al., 2007(2); Sakaguchi et al., 2007; Sakai & Tachibana, 2007; Naito et al., 2008; Sakai et al., 2010(1); Sakai et al., 2010(2)), includes novel physical aspects which have not been described in usual textbooks of plasma physics.
Also, complex dielectric constant or permittivity whose imaginary part is significantly large is observed and easily controlled in a plasma as a macroscopic value (Naito et al., 2008; Sakai et al., 2010(1)). This imaginary part strongly depends on field profiles of electromagnetic waves around plasmas when their spatial discontinuities exist, and so synthesized effects with Bloch modes in periodic structure lead to not only frequency band gap but also *attenuation* gap (Naito et al., 2008; Sakai et al., 2009). In another point of view, power dissipation due to the imaginary part leads to plasma generation (Lieberman & Lichtenberg, 1994), which is a quite nonlinear phenomenon.
In this chapter, considering the spatial discontinuities and the complex permittivity, the fundamentals of theoretical understandings on electromagnetic waves in and around plasmas are described. In Section 2.1, properties of complex permittivity are generalized using equations and a newly-developed 3-dimensional (3D) drawing. In Section 2.2, starting from the momentum equation of electrons to treat plasma effects, the complex permittivity in the Drude model is derived, and the equation is compared with that for metals whose permittivity is also in the Drude model; such a description will reveal unique features in the case of discharge plasmas for control of electromagnetic waves. In Section 3.1, various methods to describe effects of periodic spatial discontinuities are demonstrated, including both analytical and numerical ones, and specific examples of band diagrams of 2D structures are shown. In Section 3.2, another aspect of the spatial discontinuity associated with surface wave propagation is described, in which propagation of surface waves on the interface with spatial electron-density gradient is clarified. Section 4 summarizes this chapter, showing emerging aspects of electromagnetic waves in and around plasmas.

2. Fundamentals of new aspects for wave propagation

In this Section, we demonstrate features and importance of complex permittivity which is usual in a low-temperature partially-ionized plasma. Section 2.1 includes general

description which is also applicable to other lossy materials (Sakai et al., 2010(1)), and Section 2.2 focuses on the momentum balance equations of electrons in a discharge plasma, which is the origin of characteristic wave propagation in and around plasmas.

2.1 Complex permittivity in a plasma

To describe wave transmission and absorption as well as phase shift and reflection of the propagating waves, we here introduce a new drawing of dispersion relation in the 3D space of three coordinates consisting of wave frequency $\omega/2\pi$, real wavenumber k_r, and imaginary wavenumber k_i. A propagating wave which is launched at a spatial position $x=0$, or on the edge of a given media, is expressed as

$$\begin{aligned} &A(x)\exp\left(\mathrm{j}\varphi(t,x)\right) = A(x)\exp\left(\mathrm{j}(\omega t - k_r x)\right) \\ &= A_0\exp\left(k_i x\right)\exp\left(\mathrm{j}(\omega t - k_r x)\right) = A_0\exp\left(\mathrm{j}\left(\omega t - (k_r + \mathrm{j}k_i)x\right)\right), \end{aligned} \tag{2.1.1}$$

where $A(x)$ is the wave amplitude with the initial boundary condition of $A_0 = A(x=0)$, t is the time, and $\phi(t,x)$ is the phase of the wave with the initial condition of $\phi(0,0)=0$. The dispersion relation in a collisionless plasma is usually expressed in the $\omega - k_r$ plane, and we can also obtain a useful information about wave attenuation from k_i as a function of ω when significant loss or wave attenuation takes place.

Such a wave propagation in a bulk non-magnetized plasma is characterized by the permittivity ε_p in the Drude model in the form

$$\varepsilon_p = 1 - \frac{{\omega_{pe}}^2}{\omega^2(1-\mathrm{j}\nu_m/\omega)}, \tag{2.1.2}$$

where ω_{pe} is the electron plasma frequency which is a function of electron density n_e, and $\nu_m/2\pi$ is the electron elastic collision frequency. We note that, since we choose a formula in equation (2.1.1) instead of $\exp\left(\mathrm{j}(k_r x - \omega t)\right)$, the sign in the bracket of equation (2.1.2) becomes "-", and the imaginary part of the permittivity becomes negative in general (Pozar, 2005). The detailed derivation of equation (2.1.2) is given in Section 2.2. Figure 1 shows ε_p at a fixed wave frequency (4 GHz) as a function of n_e with various gas conditions on the complex plane (Sakai et al., 2010(1)). Here, we assume that the electron energy is 0.5 eV for a plasma in the afterglow and that the cross section for the electron elastic collisions is 5.0×10^{-16} cm^2 for He and 1.0×10^{-16} cm^2 for Ar from the literature (Raizer, 1991). At 760 Torr of He, $\mathrm{Re}(\varepsilon_p)$ is almost constant at unity for various n_e. On the other hand, at 5 Torr of Ar, $\mathrm{Im}(\varepsilon_p)$ is roughly zero while $\mathrm{Re}(\varepsilon_p)$ changes significantly in the negative polarity, and this feature almost corresponds to a collisionless plasma. This figure indicates that the change of gas species and pressure yields ε_p with $\mathrm{Im}(\varepsilon_p)/\mathrm{Re}(\varepsilon_p)$ ranging from 0 to infinity for $\mathrm{Re}(\varepsilon_p)<1$ on the complex plane.

Equation (2.1.2) gives us an understanding of dispersion relation in the 3D space (ω, k_r, k_i). Figure 2 displays a dispersion relation in a bulk non-magnetized plasma expressed by equation (2.1.2) (Sakai et al., 2010(1)). In the case at 5 Torr of Ar, which is nearly collisionless as mentioned earlier, the trajectory on the (ω, k_r) plane is well known in textbooks of plasma physics. The working point is always on the (ω, k_r) plane or on the (ω, k_i) plane,

which can be understood easily from equation (2.1.2). However, in the case at 120 Torr of He, the working point goes far away from the two planes below ω_{pe} and leaves a trajectory on the (k_r, k_i) plane; at such a point, the wave suffers attenuation as well as phase shift, as suggested in equation (2.1.1).
Drawings of dispersion relations in this 3D space reveal significant physical parameters of electromagnetic media, as shown in the following. Knowledge from microwave engineering (Pozar, 2005) shows that

$$k = \omega\sqrt{\mu\varepsilon}\sqrt{1 - j\frac{\sigma}{\omega\varepsilon}}, \tag{2.1.3}$$

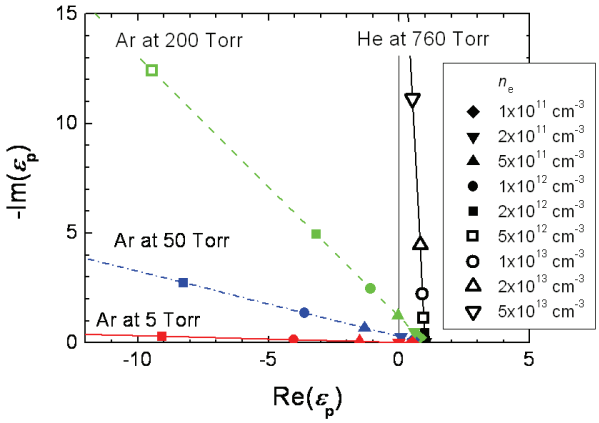

Fig. 1. Permittivity in a lossy bulk plasma with various gas condition and various n_e (Sakai et al., 2010(1)).

where ε, μ and σ is the permittivity, the permeability, and the conductivity of the media, respectively. From equation (2.1.3), the following equation is derived:

$$k_r|k_i| = \frac{\omega\mu}{2}\sigma = \frac{1}{\delta_s^{\,2}}. \tag{2.1.4}$$

Here δ_s is the skin depth of the wave into the media. $k_r|k_i|$ indicates an area on the (k_r, k_i) plane, and so a point projected on the (k_r, k_i) plane expresses conductivity of the media on the assumption that μ is constant. The inverse of the area on the (k_r, k_i) plane corresponds to square of δ_s; as the area is larger, the skin depth is shorter. Another physical parameter which is visible in this 3D drawing is the metallic/dielectric boundary. From equation (2.1.3), we also obtain

$$k_r^{\,2} - k_i^{\,2} = \omega^2\mu\varepsilon. \tag{2.1.5}$$

Comprehension of this equation gives us the following result. If $k_r > |k_i|$, ε is positive when μ is positive, leading to the fact that the media is dielectric, and if $k_r < |k_i|$, vice versa, and

we can recognize that the media is metallic. The line of $k_r = k_i$ becomes the boundary between metallic and dielectric media.

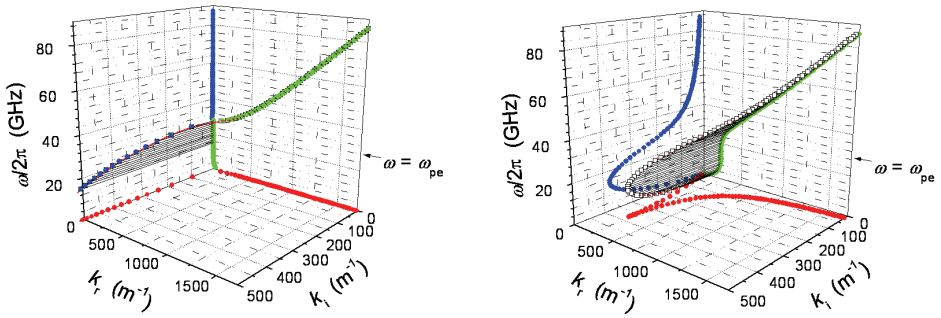

Fig. 2. Dispersion relation of electromagnetic waves in a bulk plasma with $n_e = 1 \times 10^{13}$ cm^{-3} in the 3D space. (a) In a plasma at 5 Torr of Ar gas. (b) In a plasma at 120 Torr of He gas. (Sakai et al., 2010(1)).

These characteristics arising from lossy plasmas are distinguishable from other electromagnetic media; unlike plasmas, any other material never has a variety of parameter sets such as complex $\varepsilon\,(=\varepsilon_r - \mathrm{j}\varepsilon_i)$ and σ. Such a characteristic property can be enhanced by spatial periodicity; a simple periodic ε_r distribution realized in a solid material makes a photonic or electromagnetic band material which exhibits band gaps. If we introduce the effects of ε_i by a plasma array, new features can emerge with the complex-variable effects (Naito et al., 2008; Sakai et al., 2010(2)). That is, spatial periodic change in ε_r leads to formation of frequency band gaps around which propagation-permitted frequency has a certain gap. As a novel feature in plasma cases, wave attenuation due to ε_i is significantly different between two bands above and under this band gap; we call it an *attenuation* gap. This gap arises from change of field profiles of electromagnetic waves; on the upper band, fields are localized in the lower-ε_r area, and vice versa on the lower band; such properties are demonstrated in Section 3.1.1 and 3.1.4.

2.2 Electron momentum balance equation and its effects for wave propagation

When we consider wave propagation in a plasma, the rigorous starting point of description is electron momentum balance equation. Here, a non-magnetized plasma is assumed for simplicity; if an external magnetic field is present, other terms, for instance arising from the Lorentz force, might be included. The electron momentum balance equation deals with a plasma as a kind of fluids, and it keeps good matching with macroscopic parameters such as ε and μ. Another method containing plasma effects is calculation of direct particle motion, such as a particle-in-cell simulation in which momentum balance of each single test particle is treated and collective effects of charged particles are integrated by the Poisson's equation. Another comment of our treatment based on the fluid model is that ions are assumed to be immobile due to its huge relative mass compared with electrons. Dispersion relations of some electrostatic waves propagating in a plasma such as ion acoustic waves

are derived with the effects of ion motions, although they are removed from our curiosity here.

Now, a general expression of the electron momentum balance is described as (Razer, 1991)

$$mn_{\mathrm{e}}(\boldsymbol{r})\frac{\mathrm{d}\boldsymbol{v}_{\mathrm{e}}(\boldsymbol{r})}{\mathrm{d}t} = -n_{\mathrm{e}}(\boldsymbol{r})e\boldsymbol{E}(\boldsymbol{r}) - \nabla p_{\mathrm{e}}(\boldsymbol{r}) - mn_{\mathrm{e}}(\boldsymbol{r})\boldsymbol{v}_{\mathrm{e}}(\boldsymbol{r})\nu_{\mathrm{m}}, \tag{2.2.1}$$

where t is the time, $\boldsymbol{r}$ the spatial position vector, $\boldsymbol{v}_{\mathrm{e}}$ the electron fluid velocity, m_{e} the mass of an electron, e the charge of an electron, and $\boldsymbol{E}$ the electric field. The left hand side contains a convective term arising from the change of electron position in time due to $\boldsymbol{v}_{\mathrm{e}}$ as $\mathrm{d}/\mathrm{d}t = \partial/\partial t + \boldsymbol{v}_{\mathrm{e}} \cdot \nabla$, although this term is neglected in the following. The first term on the right hand side is Coulomb force by $\boldsymbol{E}$. The second term expresses pressure-gradient term, where assumption of an isothermal plasma with a uniform spatial profile of electron temperature T_{e} enables to obtain $\nabla p_{\mathrm{e}}(\boldsymbol{r}) = kT_{\mathrm{e}}\nabla n_{\mathrm{e}}(\boldsymbol{r})$. The third term implies friction against neutral particles, i.e., change of momentum that is as frequent as ν_{m}; $\nu_{\mathrm{m}} = n_{\mathrm{g}}\langle\sigma v\rangle$, where n_{g} is the neutral gas density, σ, strongly depending of electron energy, is the cross section of the elastic collision, and $\langle\sigma v\rangle$ is a statistically averaged value over the velocity distribution.

First of all, complex permittivity of a plasma in the Drude model ε_{p}, as shown in equation (2.1.2), is derived in the following. In this case, we ignore the pressure term in equation (2.2.1) to see wave propagation in a bulk plasma. Then, current density by electrons J is given by

$$\frac{\partial \boldsymbol{J}}{\partial t} + \nu_{\mathrm{m}}\boldsymbol{J} = \varepsilon_0{\omega_{\mathrm{pe}}}^2\boldsymbol{E}. \tag{2.2.2}$$

If we express a variable $\tilde{x}(\omega)$, as a frequency spectrum at ω, via Fourier transform from $x(t)$, equation (2.2.2) becomes for a wave with frequency $\omega/2\pi$

$$(\mathrm{j}\omega + \nu_{\mathrm{m}})\tilde{\boldsymbol{J}} = \varepsilon_0{\omega_{\mathrm{pe}}}^2\tilde{\boldsymbol{E}}. \tag{2.2.3}$$

Also, one of the Maxwell equations becomes

$$\nabla \times \tilde{\boldsymbol{H}} = \mathrm{j}\omega\varepsilon_0\tilde{\boldsymbol{E}} + \tilde{\boldsymbol{J}}. \tag{2.2.4}$$

Substituting $\tilde{\boldsymbol{E}}$ in equation (2.2.3) into equation (2.2.4), we obtain ε_{p} in the following:

$$\nabla \times \tilde{\boldsymbol{H}} = \mathrm{j}\omega\varepsilon_0\tilde{\boldsymbol{E}}\left(1 - \frac{{\omega_{\mathrm{pe}}}^2}{\omega(\omega - \mathrm{j}\nu_{\mathrm{m}})}\right) = \mathrm{j}\omega\varepsilon_{\mathrm{p}}\varepsilon_0\tilde{\boldsymbol{E}}, \tag{2.2.5}$$

with the expression of ε_{p} similar to equation (2.1.2), the well known form in the Drude model. We carefully note that, from the above discussion, this form is valid for sinusoidal waves.

Secondly, we take a look on the contributions of the pressure term in equation (2.2.1). The pressure term will be significant on the edge of a plasma, and so this treatment is beneficial

when we consider wave propagation on the edge as a surface wave. Ignoring the friction term in equation (2.2.1), the current density in a plasma is given by

$$\frac{\partial \mathbf{J}}{\partial t} = \varepsilon_0 {\omega_{\mathrm{pe}}}^2 \mathbf{E} - \frac{ekT_e}{m_e} \nabla n_{\mathrm{e}}. \tag{2.2.6}$$

Then, we compare the effects of the pressure term with the cases of metals. In metal optics (Forstmann & Gerhardts, 1986), the theoretical framework similar to the fluid model in plasma physics is referred to as the hydrodynamic formulation. An expression of the current density is given as

$$\frac{\partial \boldsymbol{J}}{\partial t} = \varepsilon_0 {\omega_{\mathrm{pe}}}^2 \boldsymbol{E} - e\beta^2 \nabla n_{\mathrm{e}}. \tag{2.2.7}$$

That is, in the hydrodynamic formulation, the only different point between metals and discharge plasmas are pressure term p_{e}; in the case of metals, $p_{\mathrm{e}} = m_{\mathrm{e}}\beta^2 n_{\mathrm{e}}$ with $\beta^2 = (3/5){v_{\mathrm{F}}}^2$, where v_{F} is the Fermi velocity, and in the case of discharge plasmas $p_{\mathrm{e}} = n_{\mathrm{e}} kT_{\mathrm{e}}$. This difference comes from the state-of-phase transition at $T_{\mathrm{e}} = T_{\mathrm{F}}$ condition where the thermal energy is equal to the Fermi energy expressed by the Fermi temperature T_{F}; in the cases of metals, $T_{\mathrm{e}} < T_{\mathrm{F}}$ and metals are in the quantum phase in the category of electron gases (Isihara, 1993). In a usual metal, parameter $m_{\mathrm{e}}\beta^2$ is by 3-4 orders larger than kT_e, which yields significant differences for dispersion relations of surface wave modes between these two cases, which is discussed in Section 3.2.

3. Emerging aspects due to spatial discontinuities

3.1 Plasma periodic structure and deformation of wave propagation

Stimulated by recent progresses in photonic crystals (Yablonovitch, 2000; Noda & Baba, 2003), a number of researches have been performed about spatially periodic plasma structures which exhibit various novel phenomena that have not been expected when we use solid materials. To the best of our knowledge, the earliest publication associated with the plasma periodic structure was by Faith and Kuo (Faith et al., 1997); in their report, deformation of the band structure by rapidly generated 1D plasma structure that was analytically calculated was used for frequency upshift, and implied presence of photonic band gaps. Kalluri (Kalluri, 1998) summarized the variety of dispersion relations in the cases of both spatial and time discontinuities, and he pointed out photonic band gaps as forbidden bands. The terminology of a "plasma photonic crystal" was first announced by Hojo and Mase with its physical and technological importance (Hojo & Mase, 2004). After that, the first experimental verification of a 2D photonic crystal was performed by Sakai and his coworkers (Sakai et al., 2005(1); Sakai et al., 2005(2)), and they continued to extend their work in both theoretical and experimental results. Several groups followed these researches mainly from the theoretical points of view, as mentioned later, although Dong and her coworkers (Dong et al., 2007) performed simulated experiments of 2D plasma self-organized pattern formation, and Lo and coworkers (Lo et al., 2010) successfully observed effects for modification of propagating electromagnetic waves using metal-plasma composites.

In this section, the theoretical fundamentals for investigation of dispersion relations of plasma photonic crystals are reviewed. 1D dispersion relations are well described by the formula of a Bloch mode, given by

$$\cos ka = \cos\frac{N\omega d_{\mathrm{n}}}{c}\cos\frac{N_{\mathrm{d}}\omega d_{\mathrm{d}}}{c} - \frac{1}{2}\left(\frac{Z}{Z_{\mathrm{d}}} + \frac{Z_{\mathrm{d}}}{Z}\right)\sin\frac{N\omega d_{\mathrm{n}}}{c}\sin\frac{N_{\mathrm{d}}\omega d_{\mathrm{d}}}{c}. \tag{3.1.1}$$

Here d_{n} is the thickness of the region with N where a plasma layer is present, and c is the velocity of light. Z is the wave impedance of the equivalent slab region with the plasma structure. We also assumed that dielectric layers with refractive index N_{d}, wave impedance Z_{d}, and a thickness d_{d} were set between the plasma layers. Several authors investigated 1D plasma photonic srystals using equation (3.1.1) or other fomulae (Faith et al., 1997; Kalluri, 1998; Guo, 2009; Yin et al., 2009; Qi et al., 2010; Fan & Dong, 2010). However, for derivation of dispersion relations in 2D structures, which includes more scientific understandings as well as technical applications, several different methods have been developed, and they are described in the following.

3.1.1 Plane-wave expansion method for dispersive media

The plane-wave expansion method has been widely used to derive analytically photonic band diagrams of 2D and 3D dielectric periodic structures (Ho et al., 1990; Phihal et al., 1991). A spatially periodic permittivity, which is constant over a certain frequency range, is converted into the summation of spatial Fourier coefficients, and an assumption that multiplane-waves are superposed leads to dispersion relations by solving eigenvalue problems. That is, for the first task to use the plane-wave expansion method, we have to derive the spatial Fourier coefficients in advance, which is all right if an assumed structure is quite simple, although complicated structures are hardly treated in this procedure.

When a solid dielectric array in the plane-wave expansion method is replaced by a 2D plasma structure, the permittivity depends on ω, and the normal plane-wave expansion method is ineffective. Kuzmiak and Maradudin developed a plane-wave expansion method applicable to derivation of the photonic band structures of metallic components (Kuzmiak & Maradudin, 1997), and here we use a similar technique to solve the eigenvalue problems and further investigate cases similar to the experimental conditions (Sakaguchi et al., 2007). That is, the important point of the development of this method by Kuzmiak and Maradudin is that their formulae enable us to deal with dispersive media, or frequency-dependent permittivity, one of which is observed in a plasma in the Drude model, as shown in equation (2.1.2). Here we briefly describe this modified plane-wave expansion method introduced in (Kuzmiak & Maradudin, 1997) and followed in (Sakai et al., 2007(1)).

We set the dielectric region with permittivity ε_{d} outside the plasma column, since in experiments we frequently confine discharge gases and plasmas in a dielectric container. Using equation (2.1.2), the position vector at the site of lattice point $\boldsymbol{x}_{||}$, and translation vector $\boldsymbol{G}_{||}(=h_1\boldsymbol{b}_1 + h_2\boldsymbol{b}_2$, where $\boldsymbol{b}_1$ and $\boldsymbol{b}_2$ are the primitive translation vectors of the reciprocal lattice and h_1 and h_2 are arbitrary integers), spatially and frequency-dependent permittivity $\varepsilon(\boldsymbol{x}_{||} \mid \omega)$ in a square lattice is expressed by Fourier coefficients $\hat{\varepsilon}(\boldsymbol{G}_{||})$ as

$$\varepsilon\left(\boldsymbol{x}_{||} \mid \omega\right) = \sum_{\boldsymbol{G}_{||}} \hat{\varepsilon}\left(\boldsymbol{G}_{||}\right)\exp\left(\mathrm{j}\boldsymbol{G}_{||}\cdot\boldsymbol{x}_{||}\right) \tag{3.1.2}$$

with

$$\hat{\varepsilon}\left(\mathbf{G}_{||}\right)=\varepsilon_{\mathrm{d}}-f\left[1-\varepsilon_{\mathrm{d}}-\frac{{\omega_{\mathrm{pe}}}^2}{\omega\left(\omega-\mathrm{j}\nu_{\mathrm{m}}\right)}\right]\quad \mathrm{G}_{||}=0, \tag{3.1.3a}$$

$$\hat{\varepsilon}\left(\mathbf{G}_{||}\right)=f\left[1-\varepsilon_{\mathrm{d}}-\frac{{\omega_{\mathrm{pe}}}^2}{\omega\left(\omega-\mathrm{j}\nu_{\mathrm{m}}\right)}\right]\frac{2\mathrm{J}_1\left(\mathbf{G}_{||}R\right)}{\left(\mathbf{G}_{||}R\right)}\quad \mathrm{G}_{||}\neq 0, \tag{3.1.3b}$$

where $f=\pi R^2/a^2$ is the filling fraction and R is the radius of the cross section of a plasma column with lattice constant a. This frequency-dependent complex value of $\varepsilon(\boldsymbol{x}_{||}\,|\,\omega)$ complicates the eigenvalue problem.

From Maxwell equations with fields varying harmonically in time t in the form of $\exp(\mathrm{j}\omega t)$, we can expand the z component of the magnetic field in the TE (H polarization) mode, where the (x,y) plane exhibits the spatial periodicity of the permittivity as

$$\tilde{\boldsymbol{H}}_z\left(\boldsymbol{x}_{||}|\omega\right)=\sum_{\boldsymbol{G}_{||}}A\left(\boldsymbol{k}_{||}\middle|\boldsymbol{G}_{||}\right)\exp\left\{\mathrm{j}\left(\boldsymbol{k}_{||}+\boldsymbol{G}_{||}\right)\cdot\boldsymbol{x}_{||}\right\}. \tag{3.1.4}$$

When we substitute equation (3.1.4) into the wave equation about $\tilde{\boldsymbol{H}}_z$, coefficients $\{A(\boldsymbol{k}_{||}|\boldsymbol{G}_{||})\}$ fulfill the following equation:

$$\sum_{\boldsymbol{G}_{||}'}\left(\boldsymbol{k}_{||}+\boldsymbol{G}_{||}\right)\cdot\left(\boldsymbol{k}_{||}+\boldsymbol{G}_{||}'\right)\hat{\kappa}\left(\boldsymbol{G}_{||}-\boldsymbol{G}_{||}'\right)A\left(\boldsymbol{k}_{||}\middle|\boldsymbol{G}_{||}\right)=\frac{\omega^2}{c^2}A\left(\boldsymbol{k}_{||}\middle|\boldsymbol{G}_{||}\right), \tag{3.1.5}$$

where $\{\hat{\kappa}(\boldsymbol{G}_{||})\}$ are the Fourier coefficients of $1/\varepsilon(\boldsymbol{x}_{||}\,|\,\omega)$.

In the case of TM (E polarization) mode, the z component of electric field $\tilde{\boldsymbol{E}}_z$ is

$$\tilde{\mathbf{E}}_z\left(\mathbf{x}_{||}|\omega\right)=\sum_{\mathbf{G}_{||}}B\left(\mathbf{k}_{||}\middle|\mathbf{G}_{||}\right)\exp\left\{\mathrm{j}\left(\mathbf{k}_{||}+\mathbf{G}_{||}\right)\cdot\mathbf{x}_{||}\right\}. \tag{3.1.6}$$

Components $\{B(\boldsymbol{k}_{||}|\boldsymbol{G}_{||})\}$ fulfill the following equation as

$$\left(\boldsymbol{k}_{||}+\boldsymbol{G}_{||}\right)^2B\left(\boldsymbol{k}_{||}\middle|\boldsymbol{G}_{||}\right)=\frac{\omega^2}{c^2}\hat{\varepsilon}(\boldsymbol{0})B\left(\boldsymbol{k}_{||}\middle|\boldsymbol{G}_{||}\right)+\frac{\omega^2}{c^2}\sum_{\boldsymbol{G}_{||}'}\hat{\varepsilon}\left(\boldsymbol{G}_{||}-\boldsymbol{G}_{||}'\right)B\left(\boldsymbol{k}_{||}\middle|\boldsymbol{G}_{||}\right), \tag{3.1.7}$$

where $\sum_{\boldsymbol{G}_{||}'}$ denotes summation except for the case with $\boldsymbol{G}_{||}=\boldsymbol{G}_{||}'$.

In the process of solving equation (3.1.5) or (3.1.7), we obtain a polynomial formula for ω/c, which can be transferred to a linear problem using matrix forms. Practically, when we set a specific value of $\boldsymbol{k}$, which is a wavenumber vector composed of real numbers we obtain complex wave frequency, that is, $\omega=\omega_{\mathrm{r}}+\mathrm{j}\omega_{\mathrm{i}}$. We can plot them, as they are, as a function of $\boldsymbol{k}$, but if we convert ω_{i} to k_{i} via $\omega_{\mathrm{i}}=-v_{\mathrm{g}}k_{\mathrm{i}}$ with group velocity v_{g}, we can get a set of $(\omega(=\omega_{\mathrm{r}}),k_{\mathrm{r}},k_{\mathrm{i}})$.

Figure 3 shows a dispersion relation in 2D wavenumber, or a band diagram, of a plasma photonic crystal with a significant value of ν_{m} (Sakai et al., 2009), in which we use a 3D drawing in the $(\omega,k_{\mathrm{r}},k_{\mathrm{i}})$ space described in Section 2.1. In the $\omega-k_{\mathrm{r}}$ plane in Fig. 3, a band

gap was clearly observed from $\omega a/2\pi c$ = 0.29 to 0.32, and the dispersion relation was divided into upper and lower bands. In the lower band, there was a gap from $\omega a/2\pi c$ = 0.17 to 0.21 arising from the crossing of one flat band, but k_r and k_i were continuous on both sides of the gap. This fact indicates that this is a simple frequency band gap caused by deformation of the flat-band crossing. However, the band gap from $\omega a/2\pi c$ = 0.29 to 0.32 yielded very large differences between the upper and lower bands. Although k_r was equal on both sides at $\omega a/2\pi c$ = 0.29 and 0.32, k_i of the upper band was one order of magnitude larger than that of the lower band. The trajectory on the k_r - k_i plane clarifies that these two bands had completely different properties, and we refer it as an *attenuation* gap. This is mainly attributed to different wave-field profiles in one lattice (Sakai & Tachibana, 2007). On the upper band, wave fields concentrate on the plasma region where ε is relatively small, but on the lower band, wave fields are localized outside the plasma region where ε is relatively large. If a band gap is located above $\omega_{pe}/2\pi$, the differences in the field profile change only the matching condition between inside and outside the array region, and the band gap shows the features of a band-stop filter. On the other hand, if a band gap is located below $\omega_{pe}/2\pi$, the field profile in the periodic structure strongly affects attenuation of the propagating waves by electron elastic collisions.

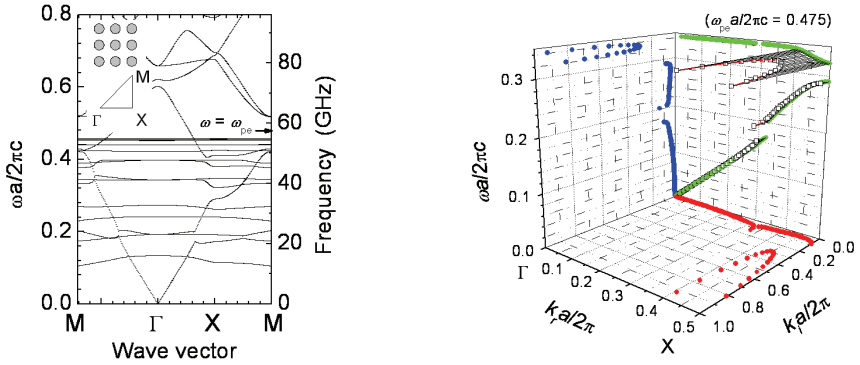

Fig. 3. (a) Dispersion relation (or band diagram) of microplasma array calculated by modified plane-expansion method. A microplasma has a diameter of 1.0 mm with lattice constant of square lattice 2.5 mm. The profile of electron density with 4×10^{13} cm^{-3} is slab shape, and the electron elastic collision frequency is set to be 0.5 ω_{pe}. (b) Dispersion relation (or band diagram) of microplasma array in 3D space with the similar parameters to those in (a). Data points of k_i at $k_i a/2\pi > 1.0$ are out of range in this figure. (Sakai et al., 2009)

3.1.2 Direct Complex-Amplitude (DCA) method

Direct numerical analysis of Maxwell equations is usually by a finite difference time-domain (FDTD) method, and it successfully gave rise to band diagrams of a 2-dimensional plasma structures as well as those of metallic photonic crystal, which is described in Section 3.1.3. What we use here to obtain band diagrams numerically is a different method dealing with the complex values of electromagnetic fields that enables us to obtain a *static* solution of the

fields in shorter central processing unit CPU time. A description of the method is found in (Sakai & Tachibana, 2006) and (Sakai et al., 2007(1)). We note that this method was originally applied to investigate wave propagation in a fusion plasma (Fukuyama et al., 1983). Here we mention its details.

From the Maxwell equations, the elimination of magnetic fields leads to a wave equation composed of electric fields $\tilde{\boldsymbol{E}}$ and external current density $\tilde{\boldsymbol{J}}_{\mathrm{ext}}$, written as

$$\nabla\times\nabla\times\tilde{\boldsymbol{E}}-\omega^2\mu\varepsilon\varepsilon_0\tilde{\boldsymbol{E}}=\mathrm{j}\omega\mu\tilde{\boldsymbol{J}}_{\mathrm{ext}}\,, \tag{3.1.8}$$

which is spatially discretized (for instance, 20×20 square meshes in one lattice) based on the finite difference method. We note that ε is expressed as $\varepsilon_{\mathrm{p}}(\omega)$ in equation (2.1.2) inside a plasma. 2D complex-value electric fields in the form expressed in equation (2.1.1) are considered, and so the TE mode in which an electric field is parallel to a 2D lattice plane can be analyzed when electric field vectors are vertical to plasma columns, in applications of the Bloch theorem to electric and magnetic (or gradient of electric) fields on the boundaries of a lattice in the form of

$$\begin{aligned}\tilde{\boldsymbol{E}}(x_0+a)&=\tilde{\boldsymbol{E}}(x_0+a)\exp(-\mathrm{j}k_x a),\\ \tilde{\boldsymbol{E}}(y_0+a)&=\tilde{\boldsymbol{E}}(y_0+a)\exp(-\mathrm{j}k_y a),\end{aligned} \tag{3.1.9}$$

and

$$\begin{aligned}\frac{\mathrm{d}\tilde{\boldsymbol{E}}}{\mathrm{d}\boldsymbol{x}}(x_0+a)&=\frac{\mathrm{d}\tilde{\boldsymbol{E}}}{\mathrm{d}\boldsymbol{x}}(x_0+a)\exp(-\mathrm{j}k_x a),\\ \frac{\mathrm{d}\tilde{\boldsymbol{E}}}{\mathrm{d}\boldsymbol{x}}(y_0+a)&=\frac{\mathrm{d}\tilde{\boldsymbol{E}}}{\mathrm{d}\boldsymbol{x}}(y_0+a)\exp(-\mathrm{j}k_y a),\end{aligned} \tag{3.1.10}$$

where (x_0, y_0) is a position vector on the boundary of lattices. In the case of the TM mode analysis, 2D magnetic field vectors will be solved numerically. From these boundary conditions, the 2D wave number of a propagating wave (k_x, k_y) is specified. The external current source is hypothetically set within a lattice. Then equation (3.1.8) is solved using the finite difference method at each discrete frequency from 0 to 150 GHz, and the local wave power density at a specific point is chosen as a cost function to detect a propagation branch. That is, when one set of frequency and wave number is matched with a propagating wave condition, the cost function represents resonance-like peaking with a very narrow frequency region (usually less than 0.1 GHz width) and with a nonlocal electric field pattern independent of the position of the hypothetical current source. On the other hand, when another set is not along the propagation branch, the electric field profile only shows a near-field pattern localized around the hypothetical current source with a very small value of the cost function value. A complex value of the electric field includes phase information, and so the wave number assumed in equations (3.1.9) and (3.1.10) can be reconfirmed by a spatially differential value of the phase $(\boldsymbol{k}\cdot\boldsymbol{x})$ at the resonance-like frequency. In this method, no derivation of a spatial Fourier coefficient is required, and so an arbitrary structure inside a lattice such as a complicated plasma shape and an arbitrary ε profile can be treated.

This method does not use time-domain discretization, unlike the FDTD method. In the case of the FDTD method, time evolution of propagating waves in media is converted into frequency spectra. To deal with the wide frequency range simultaneously, it is required to perform auxiliary calculation to reinforce the dispersive dependence of the permittivity such as shown in equation (2.2.2), and such a scheme is referred to as frequency-dependent FDTD method, which is shown in Section 3.1.3. In our method used here, a monochromatic wave at one frequency is assumed in each calculation step with a corresponding and precise value of the permittivity from equation (2.1.2). In other words, the frequency step which we set for searching wave propagation is crucial to assure the entire calculation accuracy. A narrower frequency step will yield a more accurate determination of a propagating wave, although more CPU time is required.

Using this scheme, we calculated band diagrams with $\nu_m << \omega$, that is, a collisionless case, as shown in Figs. 5-9. When ν_m is introduced as a finite value comparable to ω and ω_{pe}, note that the resonance-like frequency is searched on the complex frequency for a real wave number, like in the cases of the plane-wave expansion method described in Section 3.1.1. If we consider spatial wave damping of the static propagation in a finite region, a complex wave number is derived for a real value of frequency. This method enables us to take such a flexible approach. The relation of complex wavenumber and complex wave frequency was well investigated by Lee et al.(Lee & Mok, 2010).

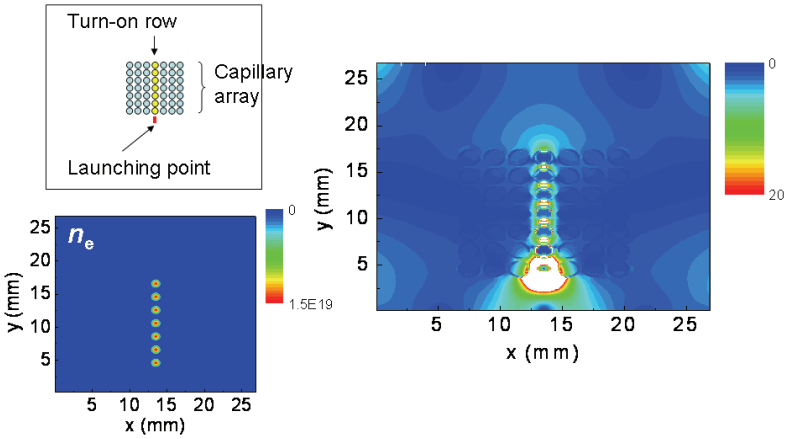

Fig. 4. 2D Wave propagation along a chain structure composed of columnar plasams at 6.2 GHz. Inset figures shows assumed configuration with assumed n_e profile in shape of 0th order Bessel function with peak density of 1.5×10^{13} cm^{-3}.

3.1.3 Finite-difference time domain method for dispersive media

In Section 3.1.2, we mentioned a different numerical method which saves computer resources, but the FDTD method is more popular and well developed if they are sufficient. We note that, even if it is possible to use the FDTD method, it provides quasi-steady solution which is difficult to be detected as a completely steady state one; human judgement will be finally required. Here, we describe the ways how the FDTD method can be applicable to analysis of wave propagation in and around plasmas.

Maxwell equations are linearized according to Yee's Algorism (Yee, 1966), as used in a conventional FDTD method. In addition, to deal with frequent-dependent permittivity equivalently, equation (2.2.2) is combined with Maxwell equations (Young, 1994) in the similar dicretization manner. Here, we ignored a pressure-gradient term from the general momentum balance equation in equation (2.2.1) because the pressure-gradient term is in the order of 10^{-7} of the right hand side of equation (2.2.2), although we have to treat it rigorously when electron temperature is quite high or when electromagnetic waves propagate with very short wavelength in the vicinity of resonance conditions. The boundary layers on the edges of the calculation area is set to be in Mur's second absorption boundary condition if the waves are assumed to be absorbed, and also we can use the Bloch or Froquet theorem described in equations (3.1.9) and (3.1.10) to assure the spatial periodic structure.

Figure 4 shows one example of the calculated results using this FDTD method. The peak n_e value in each plasma column assures the condition with $\omega < \omega_{pe}$ in which surface waves can propagate, as mentioned in Section 3.2. The launched waves from the lower side propagate along the chain structure of the isolated plasmas, and the fields are not inside plasmas but around them, similar to localized surface plasmons in the photon range along metal nanoparticles (Maier et al., 2002). That is, using this method, not only n_e profiles in one plasma but also the entire configuration surrounding plasma structures can be handled easily, although the limitation mentioned above reminds us of cross checking of the calculated results by other methods.

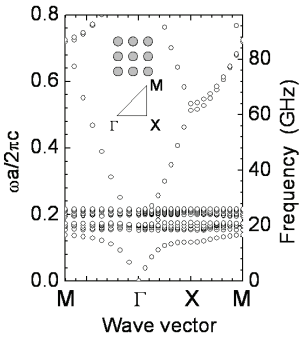

Fig. 5. Band diagram of TE mode in square lattice of plasma columns by direct complex-amplitude method. Lattice constant a is 2.5 mm. Columnar plasma with 1.75 mm in diameter is collisionless and $n_e = 10^{13}$ cm^{-3}. (Sakai & Tachibana, 2007)

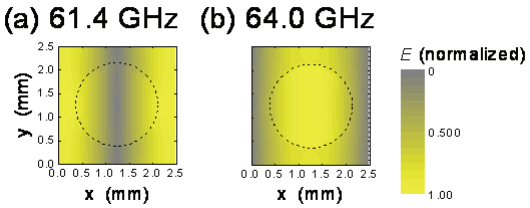

Fig. 6. Calculated profiles of electric fields normalized in amplitude in case of $k_x a/2\pi = 0.50$ and $k_y = 0$. Parameters used are similar to Fig. 5. (Sakai & Tachibana, 2007)

3.1.4 Examples of wave propagation in periodic plasma structures

Now, we demonstrate some specific examples of electromagnetic wave propagation (Sakai & Tachibana, 2007), especially with coupling of surface waves on the interface of 2-dimensional structures. The method to derive field profiles as well as band diagrams is the direct complex-amplitude (DCA) method, shown in Section 3.1.2.

Figure 5 shows a band diagram of a columnar plasma 2D array, derived by DCA method. The 2D plane was discretized into 20 × 20 meshes in one square-shaped lattice cell. This band diagram clarified typical features of 2D plasma photonic crystals, such as the band gaps, the flat bands, and the Fano mode. We also successfully obtained a case with a gradient electron density profile (Sakai et al., 2009) , in which the width of the flat band range increases due to lower density region in the periphery without changing other propagation properties; this mechanism of the wider flat band range is investigated in Section 3.2.

A unidirectional band gap in the Γ−*X* direction, which lies around 61 GHz in Fig. 5, is reviewed in the following. Forbidden propagation is enhanced due to anisotropic wave propagation in the vicinity of the band gap (Sakai et al., 2007(2)). Figure 6(a) and (b) shows the electric field profiles around the plasma columns obtained as subproducts of the band calculation shown in Fig. 5 by DCA method. The electric fields showed different patterns just below or above this band gap; their amplitude was smaller in the plasma region than in the outer area just below the band gap (61.4 GHz), but their maximum region spreads over the center of the plasma just above the band gap (64.0 GHz). These structures were similar to 1D standing waves, and effects of the plasma with circular cross section were ambiguous.

Next, we focus on properties of the flat bands. As shown in Figs. 3 and 5, the flat bands with very low group velocity region are present below $\omega_{pe}/2\pi$ = 28.4 GHz. Such a wide frequency range arises from both localized surface modes and their periodicity.

Surface modes around a metal particle were well investigated in the photon frequency range (Forstmann & Gerhardts, 1986). When electromagnetic waves encounter an individual metal particle smaller than the wavelength, they are coupled with localized surface modes called "surface plasmon polalitons." Their maximum frequency spectrum is at $\omega_{pe}/\sqrt{(1+\varepsilon_d)}$, where ε_d is the permittivity of the dielectric medium surrounding the metal particle. The localized surface modes have azimuthal (angular) mode number l around the particle, and l becomes larger as the frequency approaches $\omega_{pe}/\sqrt{(1+\varepsilon_d)}$, which corresponds to ~20 GHz in Fig. 5.

In our case, however, structure periodicity complicates the problem. Recently, several reports about metallic photonic crystals (Kuzmiak & Maradudin, 1997; Ito & Sakoda, 2001; Moreno et al., 2002; Torder & John, 2004; Chern et al., 2006) have dealt with this issue. We investigated the electric field profiles calculated by DCA method along the band branches to clarify the roles of surface plasmons and their periodic effects. Figure 7 shows several amplitude profiles of electric fields in the propagating waves in the 2D columnar plasmas, with the same parameters as Figs. 5 and 6.

Electric fields in the Fano mode, present below the flat band region, are shown in Fig. 7(a). The amplitude of the electric field inside the columnar plasma was very small, and most of the wave energy was uniformly distributed and flowed outside the plasma. As we mentioned earlier, this wave branch coalesces with the flat bands at their lowest frequency as the frequency increases.

Electric fields of the waves on flat bands are shown in Fig. 7(b)–(h). A clearly different point from Fig. 7(a) is that the electric fields were localized on the boundary between the plasma

and the vacuum. Another unique feature was the change of l of the standing waves around the plasma column. At lower frequency, l around the plasma column was low, and it became multiple at a higher frequency. This tendency is consistent with the general phenomena of surface plasmons around a metal particle. The highest l number (~6) was observed around 20 GHz, as shown in Fig. 7(e), and this frequency was approximately in the condition of $\omega_{pe}/\sqrt{2}$ which agrees with the predicted top frequency of the surface plasmon around a metal sphere ($\omega_{pe}/\sqrt{(1+\varepsilon_d)}$ in the case where the surrounding medium is a vacuum ($\varepsilon_d = 1$)).

However, the sequence of l along the frequency axis was not perfect for the surface waves around an individual metal sphere in the array. Above 20 GHz in Figs. 5 and 7 there are some flat bands, separated from the group below 20 GHz. In this group, however, no sequential change of l was found in Fig. 7. This might arise from the periodicity, as suggested by Ito and Sakoda (Ito & Sakoda, 2001). That is, Fig. 7(f)–(h) shows a different tendency from that below 20 GHz, and these electric field profiles imply that surface wave modes are localized in the gap region of the adjacent plasma columns and no boundary condition for standing waves around the column affects them. Note that this group of the flat bands above 20 GHz was hardly detected using the modified plane-wave method described in Section 3.1.1, as shown in Ref. (Sakai & Tachibana, 2007), where the region with no detection of flat bands ranges from 20 GHz to $\omega_{pe}/2\pi$. The structures of wave propagation are too fine to be detected in the modified plane-wave method, and therefore, an increase of assumed plane waves might be required to detect them in this method.

In summary, wave propagation on the flat bands of a 2-D columnar plasma array is mainly attributed to the dispersion of the localized surface modes around an individual columnar plasma and is modified by periodicity in the plasma array. These phenomena analogically resemble light waveguides composed of metal nanoparticle chains (Maier et al., 2002). The property observed in the aforementioned calculations will be applied to the dynamic waveguide of the electromagnetic waves composed of localized surface modes, similar to that shown in Fig. 4, since flat bands can intersect with the wave branches with various characteristic impedances.

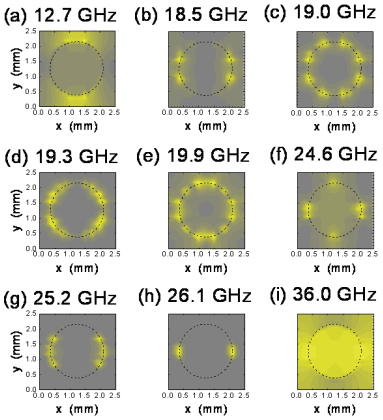

Fig. 7. Calculated profiles of electric fields normalized in amplitude in case of $k_x a/2\pi = 0.25$ and $k_y = 0$. Parameters used are similar to Fig. 5. (Sakai & Tachibana, 2007)

So far, we have investigated wave propagation in an array of plasma columns. The next target is antiparallel structure, which is an infinite-size plasma with periodic *holes*. Above $\omega_{pe}/2\pi$, periodic dielectric constant in space will contribute to form a similar band diagram. When the frequency is low enough, since there is no continuous vacuum space in this structure, wave propagation below $\omega_{pe}/2\pi$ is considered difficult from the first guess of the wave-propagation theory in a bulk plasma.

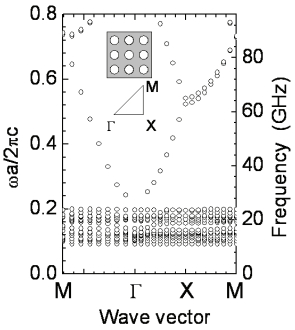

Fig. 8. Band diagram of TE mode in square lattice of plasma holes by direct complex-amplitude method. Lattice constant a is 2.5 mm. Circular holes with 1.75 mm in diameter are in a collisionless infinite plasma with $n_e = 10^{13}$ cm^{-3}. (Sakai & Tachibana, 2007)

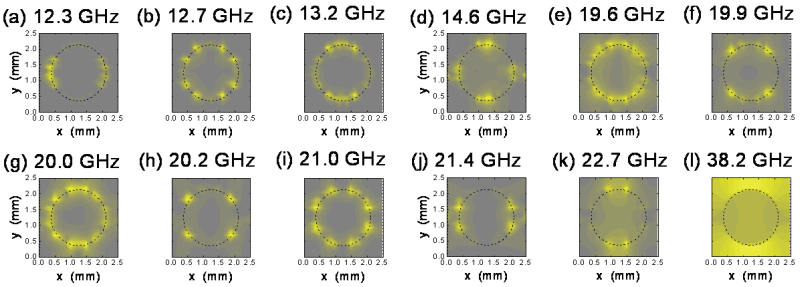

Fig. 9. Calculated profiles of electric fields normalized in amplitude in case of $k_x a/2\pi = 0.25$ and $k_y = 0$. Parameters used are similar to Fig. 8. (Sakai & Tachibana, 2007)

A band diagram of the infinite plasma with periodic holes, calculated by DCA method, is shown in Fig. 8. The basic features are common to the diagram in Fig. 5, and several different points from Fig. 5 can be found in Fig. 8. The first band-gap frequency in the $\Gamma - X$ direction was slightly higher, since the filling fraction of the plasma region in one lattice cell in Fig. 8 (0.62) was larger than that in Fig. 5 (0.38) and it reduced the synthetic dielectric constant above $\omega_{pe}/2\pi$. No Fano mode was present in the low frequency region since there was no continuous vacuum region. Note that wave propagation remained below $\omega_{pe}/2\pi$ and the flat band region expanded to lower frequencies, which are examined in the following.

Figure 9 shows the electric field profiles in one lattice cell at various frequencies. In this case, no clear dependence of the azimuthal mode number l on the frequency was found; for instance, l = 1 at 12.3 GHz, l = 4 at 12.7 GHz, and l = 2 at 14.6 GHz. The path for the wave

energy flow is limited to four points from the adjacent lattice cells through the short gap region between holes, and a plasma hole works as a wave cavity. Furthermore, conditions for standing eigenmodes along the inner surface of the hole are also required. In contrast, in the case of the columnar plasmas in Fig. 7, wave energy freely flows around the column, and therefore, wave patterns fulfill eigenmode conditions around the plasma columns and their periodicity. These facts yield differences between the cases of columnar plasmas and plasma holes.

It is difficult to express the penetration depth of the electromagnetic waves in surface plasmon in a simple formula (Forstmann & Gerhardts, 1986), but here, for the first approximation, we estimate usual skin depth δ_s on the plasma surface with a slab n_e profile instead. We use the well-known definition in a collisionless plasma as $\delta_s = c/\omega_{pe}$, where c is the velocity of light, and δ_s is 1.7 mm using the assumed n_e value in the aforementioned calculation as 10^{13} cm^{-3}. Since this value is comparable to the size and the gap of the plasma(s) in the aforementioned calculation, no wave propagation is expected in the normal cases in the cutoff condition. That is, wave propagation in the case of the hole array is supported not only by tunnelling effects but also by resonant field enhancement on the boundary that can amplify the local fields that strongly decay in the plasma region but couple with those in adjacent cells as near fields.

Using metals and waves in the photon range, similar phenomena will be found when holes are made in the 2-D lattice structure in the bulk metal, and waves propagate along this 2-D plane. In that case, some amount of light will pass through the metal in the usual cutoff condition; *opaque* material will become *transparent* to a certain extent, although damping by electron collisions will be present in the actual metallic materials.

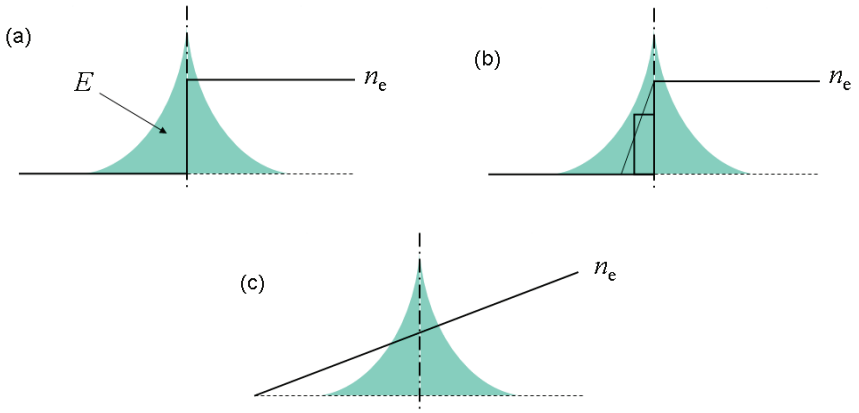

Fig. 10. Schematic view of surface waves on various models. (a) Model for ideal metal surface. (b) Bulk selvage model for metal surface. (c) Model for a discharge plasma.

3.2 Surface wave propagation in a plasma with spatially gradient electron density

In Section 3.1.4, several features of the localized surface waves in plasma periodic structures have been demonstrated. Some features are in common with the cases of light propagation on metal particles, but others are not; in this section, we clarify the different points from the surface waves or the surface plasmon polaritons on metal surfaces.

Figure 10 displays schematic views of surface waves and n_e profiles in both plasma and metal cases. In most cases of metal surfaces, since a n_e profile is almost similar to a slab shape, analysis of surface waves is rather easy, and surface plasmon polaritons have been well understood so far. On the other hand, in the plasma case, characteristic length of n_e is much larger than the presence width of the density gradient. This point is identical to plasma surface waves, although rigorous reports of these waves have been very few (Nickel et al., 1963; Trivelpiece & Gould, 1959; Cooperberg, 1998; Yasaka & Hojo, 2000). Here, we describe these waves using analytical approaches (Sakai et al., 2009).

The plasma is assumed to be infinite in the half space for the spatial coordinate $z < 0$ with vacuum region for $z > 0$. Since we deal with wave propagation, a variable x has two components as

$$x = x_0 + x_1, \tag{3.2.1}$$

where subscripts 0 and 1 correspond to static and fluctuating (wave-field) parts, respectively, equation (2.2.6) in the fluid or the hydrodynamic model is rewritten as

$$\frac{\partial \boldsymbol{J}_1(z)}{\partial t} = \varepsilon_0 \omega_{\mathrm{pe0}}(z)^2 \boldsymbol{E}_1(z) - \frac{ekT_e}{m} \nabla n_{\mathrm{e1}}(z). \tag{3.2.2}$$

Here, Poisson's equation given as

$$\nabla^2 \varphi_1(z) = -\rho_1 / \varepsilon_0 \tag{3.2.3}$$

with $\boldsymbol{E}_1 = -\nabla \varphi_1$ and continuity equation given as

$$\nabla \cdot \boldsymbol{J}_1 + \mathrm{d}\rho_1 / \mathrm{d}t = 0 \tag{3.2.4}$$

are coupled with equation (3.2.2), where φ is the electric potential and ρ the amount of charge. We also assume electron temperature $T_e = 1$ eV as a constant value. To make it possible to obtain an analytical solution, a specific n_e profile is assumed as

$$\omega_{\mathrm{pe0}}(z)^2 = \omega_{\mathrm{pe0}}(-\infty)^2 \left(1 - \cosh^{-2}(\alpha_1 z)\right)$$

for $z < 0$ and $\omega_{\mathrm{pe0}}(z)^2 = 0$ for $z \geq 0$, in the similar manner to the previous studies (Eguiluz & Quinn, 1976; Sipe, 1979), where α_1 represents density gradient factor, and solutions are derived using the similar method in Ref. (Sipe, 1979).

Here we point out common and different properties between metals and plasmas deduced from this model. Figure 11(a) shows analytical dispersion relations including two lowest-order multipole modes on a plasma half space with n_e gradient region characterized by $\alpha_1 = 40$ cm^{-1}, where ω_n is the eigen frequency of the multipole mode number n. There should be a number of multipole modes with every odd number n, and the two lowest cases ($n = 1$ and 3) are displayed in Fig. 11(a). Higher multiple modes can exist as long as the density decay region works as a resonance cavity. A branch similar to the ordinary surface plasmon with the resonance frequency of $\omega_{\mathrm{sp}} = \omega_{\mathrm{pe}} / \sqrt{2}$ is observed, and the two multipole modes are located at much lower frequencies than ω_{sp}.

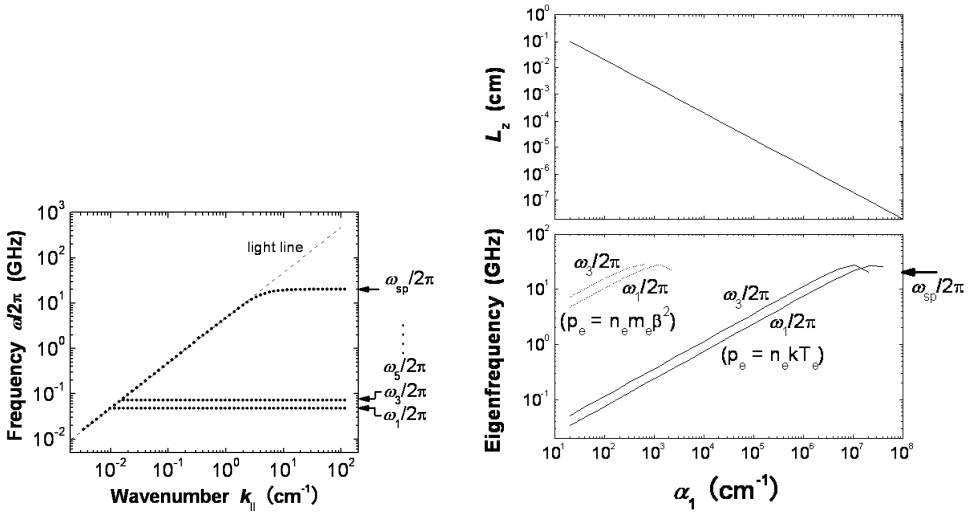

Fig. 11. Analytically calculated dispersion relations of surface waves propagating along a surface of a plasma half space with a gradual electron density profile. (a) Dispersion relations with α_1 = 40 cm^{-1} and $\omega_{pe}/2\pi \sim 28$ GHz. (b) Dependence of gradient parameter α_1 on length of density gradient L_z in the top figure and eigenfrequencies of the two lowest order in the bottom figure. Eigenfrequencies are plotted for two different pressure terms.

As previously described in Section 2.2, in a usual metal, parameter $m\beta^2$ is much larger than kT_e, which yields significant differences for dispersion relations of surface wave modes between plasma and metal cases. One of them is expressed in Fig. 11(b), which indicates the difference of frequency region of the surface wave modes. The top figure of Fig. 11(b) shows approximate length of gradient region L_z as a function of the parameter α_1. From the bottom part of Fig. 11(b), at one value of α_1, the frequency range of the surface wave modes (from ω_1 to ω_{sp}) in the case of gas-discharge plasmas is much larger than that in the case of metals with $\beta = 0.85 \times 10^8$ cm/sec. That is, not only inherent density gradient on the edge but also accelerating factor by the difference of the pressure term widens frequency region of the surface wave modes in a gas-discharge plasma.

Up to now, we have concentrated on surface waves on an infinite flat interface. Usually the excitation of surface waves on such a flat surface requires some particular methods such as ATR configuration or periodic structure like fluctuating surface. If we generate an isolated plasma from the others whose size is less than the wavelength, localized surface waves can be excited through electromagnetic waves in a free space, as shown in Section 3.1.4. In this case, we also observe similar wave propagation in comparison with the case of the flat surface (Sakai et al., 2009); the spectra of the waves propagating along the chain structure of the isolated plasmas with spatial n_e gradient are much wider than that without the density gradient. That is, using such inherent property of the density gradient with the pressure term determined by electron temperature, we expect a very wide range waveguide composed of plasma chains; an example was demonstrated in Fig. 4.

Figure 12 shows conceptual dispersion relations of surface wave modes on surfaces of isolated plasmas, as a summary of the discussion here. In a case of the gradual profile of n_e shown in Fig. 12(a), the propagating modes are on $\omega - z$ plane. Wave fields are distributed around the condition of $\varepsilon = 0$, i.e., on the layer with $\omega = \omega_{pe}$, and localized in a narrower region whose width is less than δ_s. Their frequency region is very wide and the surface modes can be present at frequencies much lower than $\omega_{pe}(0)$ by one or two orders. On the other hand, In a case of the slab profile of n_e shown in Fig. 12(b), the propagating modes are on $\omega - \varepsilon$ plane with narrow permittivity region (e.g., $-2 < \varepsilon < -1$). Wave fields are distributed around a surface of solids, i.e., $z = 0$ in Fig. 12(b), where n_e is discontinuous, and expand in a spatial range approximately equal to δ_s. Such newly-verified features of surface wave modes on small gas-discharge plasmas will open new possibilities of media for electromagnetic waves such as plasma chains demonstrated in Fig. 4 and spatially narrow waveguide on a n_e-gradient plasma surface.

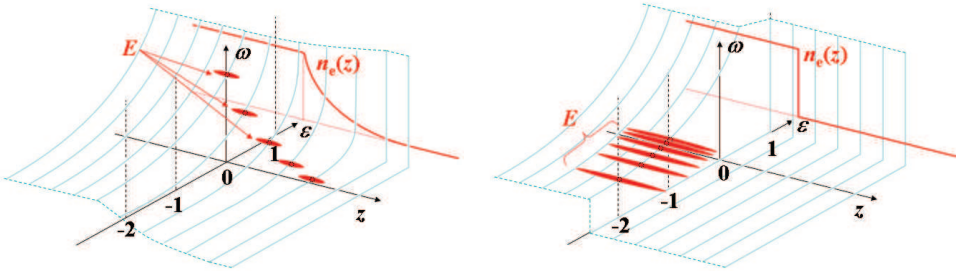

Fig. 12. Summary of dispersion relations of surface wave modes with two different electron density profiles. (a) Case of a gradual density profile. (b) Case of a slab density profile.

4. Concluding remarks

In this chapter, we investigate emerging features of electromagnetic wave propagation when we consider spatial structures of plasmas with complex permittivity. We derived the complex permittivity and introduce its drawing technique. We also obtained several methods to derive propagation of waves in two-dimensional plasma structures, and analytical solution of surface waves with the effects of significant n_e gradient. Combining these results, we verified wave propagation as localized surface modes. Clearly, the properties of wave propagation are different from those of surface waves on metals as well as those in waves propagating solid photonic crystals. These fundamentals will be applicable to various physical approaches as well as technological applications for control of electromagnetic waves.

5. References

Chern, R.L., Chang, C.C. & Chang, C.C. (2006). Analysis of surface plasmon modes and band structures for plasmonic crystals in one and two dimensions, *Phys. Rev. E*, vol. 73: 036605-1-15

Cooperberg, D. J. (1998). Electron surface waves in a nonuniform plasma lab, *Phys. Plasmas*, Vol. 5: 862-872

Dong, L., He Y., Liu, W., Gao R., Wang, H. & Zhao, H. (2007). Hexagon and square patterned air discharges, *Appl. Phys. Lett.* Vol. 90: 031504-1-3

Eguiluz, A. & Quinn, J. J. (1976). Hydrodynamic model for surface plasmons in metals and degenerate semiconductor, *Phys.Rev. B,* Vol. 14: 1347-1361

Faith, J., Kuo, S.P. & Huang, J. (1997). Frequency downshifting and trapping of an electromagnetic wave by a rapidly created spatially periodic plasma *Phys. Rev. E,* Vol. 55: 1843-1851

Fan W. & Dong L. (2010). Tunable one-dimensional plasma photonic crystals in dielectric barrier discharge, *Phys. Plasmas,* Vol. 17: 073506-1-6

Forstmann, F. & Gerhardts, R. R. (1986). *Metal Optics Near the Plasma Frequency,* Springer-Verlag, Berlin

Fukuyama, A., Goto, A., Itoh, S.I. & Itoh, K. (1983). Excitation and Propagation of ICRF Waves in INTOR Tokamak, *Jpn. J. Appl. Phys.*, Vol. 23: L613-L616

Ginzburg, V.L. (1964). *The Propagation of Electromagnetic Waves in Plasma,* Pergamon Press, Oxford

Guo, B. (2009). Photonic band gap structures of obliquely incident electromagnetic wave propagation in a one-dimension absorptive plasma photonic crystal, *Phys. Plasmas,* Vol. 16: 043508-1-6

Ho, K.M., Chan, C.T. & Soukoulis, C.M. (1990). Existence of a photonic gap in periodic dielectric structures, *Phys. Rev. Lett.* Vol. 65: 3152-3155

Hojo, H. & Mase A. (2004). Dispersion relation of electromagnetic waves in one-dimensional plasma phonic crystals, *J. Plasma Fusion Res.* Vol. 80: 89-90.

Isihara, A. (1993). *Electron Liquids,* Springer-Verlag, Berlin

Ito, T. & Sakoda, K. (2001). Photonic bands of metallic systems. II. Features of surface plasmon polaritons, *Phys. Rev. B,* vol. 64: 045117-1-8

Kalluri, D.K. (1998). *Electromagnetics of Complex Media,* CRC Press, Boca Raton

Kuzmiak, V. & Maradudin, A.A. (1997). Photonic band structures of one- and two-dimensional periodic systems with metallic components in the presence of dissipation, *Phys. Rev. B* Vol. 55: 7427-7444

Lee, H.I. & Mok, M. (2010). On the cubic zero-order solution of electromagnetic waves. I. Periodic slabs with lossy plasmas, *Phys. Plasmas,* Vol. 17: 072108-1-9

Lieberman, M.A. & Lichtenberg, A.J. (1994). *Principles of Plasma Discharges and Materials Processing,* John Wiley & Sons, New York

Lo, J., Sokoloff, J., Callegari, Th., & Boeuf, J.P. (2010). Reconfigurable electromagnetic band gap device using plasma as a localized tunable defect, *Appl. Phys. Lett.* Vol. 96: 251501-1-3

Maier, S.A., Brongersma, M.L., Kik, P.G. & Atwater, H.A. (2002). Observation of near-field coupling in metal nanoparticle chains using far-field polarization spectroscopy, *Phys. Rev. B*, vol. 65: 193408-1-4

Moreno, E., Erni, D. & Hafner, C. (2002). Band structure computations of metallic photonic crystals with the multiple multipole method, *Phys. Rev. B,* vol. 65: 155120-1-10

Naito, T., Sakai, O. & Tachibana, K. (2008). Experimental verification of complex dispersion relation in lossy photonic crystals, *Appl. Phys.Express* Vol. 1: 066003-1-3.

Nickel, J. C., Parker, J. V. & Gould, R. W. (1963). Resonance Oscillations in a Hot Nonuniform Plasma Column, *Phys. Rev. Lett.* Vol. 11: 183-185.

Nishikawa, K. & Wakatani, M. (1990). *Plasma Physics,* Aspringer-Verlag, Berlin

Noda, S. & Baba T. (ed.) (2003). *Roadmap on Photonic Crystals*, Kluwer Academic, Boston

Phihal, M., Shambrook, A., Maradudin, A.A. (1991) and P. Sheng, Two-dimensional photonic band structure, *Opt. Commun.* Vol. 80: 199-204

Pozar, D.M. (2005). *Microwave Engineering (3rd ed.),* John Wiley & Sons, Hoboken

Qi, L., Yang, Z., Lan, F., Gao, X. & Shi, Z. (2010). Properties of obliquely incident electromagnetic wave in one-dimensional magnetized plasma photonic crystals, *Phys. Plasmas,* Vol. 17: 042501-1-8

Razer, Y. P. (1991). *Gas Discharge Physics,* Springer-Verlag, Berlin

Sakaguchi, T., Sakai, O. & Tachibana, K. (2007). Photonic bands in two-dimensional microplasma arrays. II. Band gaps observed in millimeter and sub-terahertz ranges, *J. Appl. Phys.* Vol. 101: 073305-1-7

Sakai, O., Sakaguchi, T. & Tachibana, K. (2005(1)). Verification of a plasma photonic crystal for microwaves of millimeter wavelength range using two-dimensional array of columnar microplasmas, *Appl. Phys. Lett.* Vol. 87: 241505-1-3

Sakai, O., Sakaguchi, T., Ito, Y. & Tachibana, K. (2005(2)). Interaction and control of millimetre-waves with microplasma arrays, *Plasma Phys. Contr. Fusion* Vol. 47: B617-B627

Sakai, O. & Tachibana, K. (2006). Dynamic control of propagating electromagnetic waves using tailored millimeter plasmas on microstrip structures, *IEEE Trans. Plasma Sci.,* vol. 34: 80-87

Sakai, O., Sakaguchi, T. & Tachibana, K. (2007). Photonic bands in two-dimensional microplasma arrays. I. Theoretical derivation of band structures of electromagnetic waves, *J. Appl. Phys.* Vol. 101: 073304-1-9

Sakai, O., Sakaguchi T. & Tachibana K. (2007(2)). Plasma photonic crystals in two-dimensional arrays of microplasmas, *Contrib. Plasma Phys.*, vol. 47: 96-102

Sakai, O. & Tachibana, K. (2007). Properties of electromagnetic wave propagation emerging in two-dimensional periodic plasma structures, *IEEE Trans. Plasma Sci.* Vol. 35:1267-1273.

Sakai, O., Naito, T. & Tachibana K. (2009). Microplasma array serving as photonic crystals and Plasmon Chains, *Plasma Fusion Res.* Vol. 4: 052-1-8.

Sakai, O., Naito, T. & Tachibana, K. (2010(1)). Experimental and numerical verification of microplasma assembly for novel electromagnetic media, *Physics of Plasmas*, vol. 17: 057102-1-9.

Sakai, O., Shimomura, T. & Tachibana, K. (2010(2)). Microplasma array with metamaterial effects, *Thin Solid Films*, vol. 518: 3444-3448

Sipe, J. E. (1979). The ATR spectra of multipole surface plasmons, *Surf. Sci.,* Vol. 84: 75-105

Stix, T.H. (1962). *The Theory of Plasma Waves,* McGraw-Hill, New York

Swanson, D.G. (1989). *Plasma Waves,* Academic Press, Boston

Toader, O. & John, S. (2004). Photonic band gap enhancement in frequency-dependent dielectrics, *Phys. Rev. E,* vol. 70: 046605-1-15

Trivelpiece, A. W. & Gould, R. W. (1959). Surface charge waves in cylindrical plasma columns, *J. Appl. Phys.,* Vol. 30: 1784-1793

Yablonovitch, E. (2000), How to be truly photonic, *Science* Vol. 289, 557-559.

Yasaka, Y. & Hojo, H. (2000). Enhanced power absorption in planar microwave discharges, *Phys. Plasmas,* Vol. 7: 1601-1605

Yee, K. (1966). Numerical solution of initial boundary value problems involving maxwell equations in isotropic media, *IEEE Trans. Antennas Propag.*, Vol. 14: 302-307

Yin, Y., Xu, H., Yu, M.Y., Ma, Y.Y., Zhuo, H.B., Tian, C.L. & Shao F.Q. (2009). Bandgap characteristics of one-dimensional plasma photonic crystal, *Phys. Plasmas,* Vol. 16: 102103-1-5

Young, J.L. (1994). A full finite difference time domain implementation for radio wave propagation in a plasma, *Radio Sci.,* Vol. 29: 1513-1522

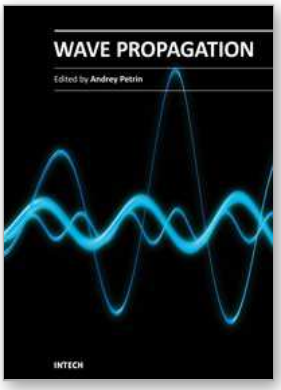

Wave Propagation
Edited by Dr. Andrey Petrin

ISBN 978-953-307-275-3
Hard cover, 570 pages
Publisher InTech
Published online 16, March, 2011
Published in print edition March, 2011

The book collects original and innovative research studies of the experienced and actively working scientists in the field of wave propagation which produced new methods in this area of research and obtained new and important results. Every chapter of this book is the result of the authors achieved in the particular field of research. The themes of the studies vary from investigation on modern applications such as metamaterials, photonic crystals and nanofocusing of light to the traditional engineering applications of electrodynamics such as antennas, waveguides and radar investigations.

How to reference
In order to correctly reference this scholarly work, feel free to copy and paste the following:

Osamu Sakai (2011). Propagation of Electromagnetic Waves in and around Plasmas, Wave Propagation, Dr. Andrey Petrin (Ed.), ISBN: 978-953-307-275-3, InTech, Available from: http://www.intechopen.com/books/wave-propagation/propagation-of-electromagnetic-waves-in-and-around-plasmas

INTECH
open science | open minds

InTech Europe
University Campus STeP Ri
Slavka Krautzeka 83/A
51000 Rijeka, Croatia
Phone: +385 (51) 770 447
Fax: +385 (51) 686 166
www.intechopen.com

InTech China
Unit 405, Office Block, Hotel Equatorial Shanghai
No.65, Yan An Road (West), Shanghai, 200040, China
中国上海市延安西路65号上海国际贵都大饭店办公楼405单元
Phone: +86-21-62489820
Fax: +86-21-62489821